

See discussions, stats, and author profiles for this publication at: <https://www.researchgate.net/publication/309550052>

Far-field pressurization likely caused one of the largest injection induced earthquakes by reactivating a large pre-existing...

Data · October 2016

CITATIONS

0

READS

33

8 authors, including:



[William Luther Yeck](#)

United States Geological Survey

23 PUBLICATIONS 105 CITATIONS

[SEE PROFILE](#)



[Matthew Weingarten](#)

Stanford University

17 PUBLICATIONS 221 CITATIONS

[SEE PROFILE](#)



[Eric A. Bergman](#)

Global Seismological Services

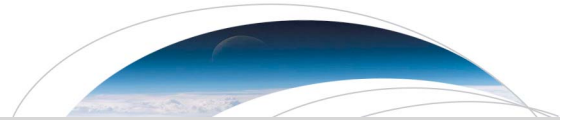
82 PUBLICATIONS 2,543 CITATIONS

[SEE PROFILE](#)

Some of the authors of this publication are also working on these related projects:



A Global Catalog of Calibrated Earthquake Locations [View project](#)



RESEARCH LETTER

10.1002/2016GL070861

Key Points:

- One of the largest injection-related earthquakes was likely induced by far-field pressurization near Fairview, Oklahoma
- Earthquakes occur in Precambrian basement, 6–10 km below sea level, on a partially unmapped fault
- Observations point to the critical role optimally oriented preexisting faults play in the occurrence of large induced earthquakes

Supporting Information:

- Supporting Information S1

Correspondence to:

W. L. Yeck,
wyeck@usgs.gov

Citation:

Yeck, W. L., M. Weingarten, H. M. Benz, D. E. McNamara, E. A. Bergman, R. B. Herrmann, J. L. Rubinstein, and P. S. Earle (2016), Far-field pressurization likely caused one of the largest injection induced earthquakes by reactivating a large preexisting basement fault structure, *Geophys. Res. Lett.*, *43*, doi:10.1002/2016GL070861.

Received 16 AUG 2016

Accepted 25 SEP 2016

Accepted article online 27 SEP 2016

Far-field pressurization likely caused one of the largest injection induced earthquakes by reactivating a large preexisting basement fault structure

W. L. Yeck¹, M. Weingarten², H. M. Benz¹, D. E. McNamara¹, E. A. Bergman³, R. B. Herrmann⁴, J. L. Rubinstein⁵, and P. S. Earle¹

¹U.S. Geological Survey, National Earthquake Information Center, Golden, Colorado, USA, ²Department of Geophysics, Stanford University, Stanford, California, USA, ³Global Seismological Services, Golden, Colorado, USA, ⁴Department of Earth and Atmospheric Sciences, Saint Louis University, Saint Louis, Missouri, USA, ⁵U.S. Geological Survey Earthquake Science Center, Menlo Park, California, USA

Abstract The M_w 5.1 Fairview, Oklahoma, earthquake on 13 February 2016 and its associated seismicity produced the largest moment release in the central and eastern United States since the 2011 M_w 5.7 Prague, Oklahoma, earthquake sequence and is one of the largest earthquakes potentially linked to wastewater injection. This energetic sequence has produced five earthquakes with M_w 4.4 or larger. Almost all of these earthquakes occur in Precambrian basement on a partially unmapped 14 km long fault. Regional injection into the Arbuckle Group increased approximately sevenfold in the 36 months prior to the start of the sequence (January 2015). We suggest far-field pressurization from clustered, high-rate wells greater than 12 km from this sequence induced these earthquakes. As compared to the Fairview sequence, seismicity is diffuse near high-rate wells, where pressure changes are expected to be largest. This points to the critical role that preexisting faults play in the occurrence of large induced earthquakes.

1. Introduction

Since the early 2000s, the rate of earthquakes in the central United States (CUS) has dramatically increased and has been documented to be largely anthropogenic [Ellsworth, 2013; Weingarten et al., 2015]. Many recent CUS earthquake sequences have been linked to wastewater disposal [e.g., Keranen et al., 2013; Kim, 2013; Rubinstein et al., 2014; Yeck et al., 2016], while a limited number of sequences have been linked to hydraulic fracturing operations [e.g., Holland, 2013a; Friberg et al., 2014; Skoumal et al., 2015]. In Oklahoma, the link between wastewater injection and seismicity is well documented [Keranen et al., 2014; Walsh and Zoback, 2015] and includes many notable sequences [see McNamara et al., 2015a]. For example, the 2011 Prague M_w 5.7 earthquake, one of the largest historical earthquakes in Oklahoma, resulted in structural damage and injuries and was linked to wastewater disposal [Ellsworth, 2013; Keranen et al., 2013; Sumy et al., 2014; McNamara et al., 2015a]. The October 2014 Cushing sequence, which included two $M_w \geq 4$ earthquakes, had high correlation between daily wastewater injection volumes and daily seismicity and occurred beneath the largest oil storage facility in the United States [McNamara et al., 2015b]. The hazard imposed by these induced earthquakes can change rapidly [Petersen et al., 2016]; therefore, it is critical to rapidly and accurately document potentially induced sequences.

On 13 February 2016, a M_w 5.1 earthquake ruptured near Fairview, Oklahoma, southwest of a series of high-rate (>300,000 barrels (bbls)/month) wastewater disposal wells (Figure 1). This was the largest earthquake in the central and eastern United States since the 2011 M_w 5.7 Prague Oklahoma earthquake and is one of the largest earthquakes in the Oklahoma historical record. Other moderate (M 5–6) Oklahoma earthquakes include the 2016 M_w 5.8 Pawnee earthquake and potentially the estimated M 4.8– M 5.7 1952 El Reno and the estimated M 4.9–5.7 1882 Fort Gibson earthquakes [Frohlich and Davis, 2002; Holland et al., 2013b; Petersen et al., 2014; Hough and Page, 2015].

The Fairview main shock was felt throughout the CUS, with weak shaking reported at distant urban centers including Dallas, Texas, and Kansas City, Missouri, and maximum reported U.S. Geological Survey (USGS) ‘Did You Feel It’ intensities of VII (very strong shaking) in the epicentral region (see acknowledgments and data). This sequence included five M_w 4 or greater earthquakes prior to the M_w 5.1 main shock and represents a major component of the total moment release in Oklahoma and Kansas since the increased rate of anthropogenic

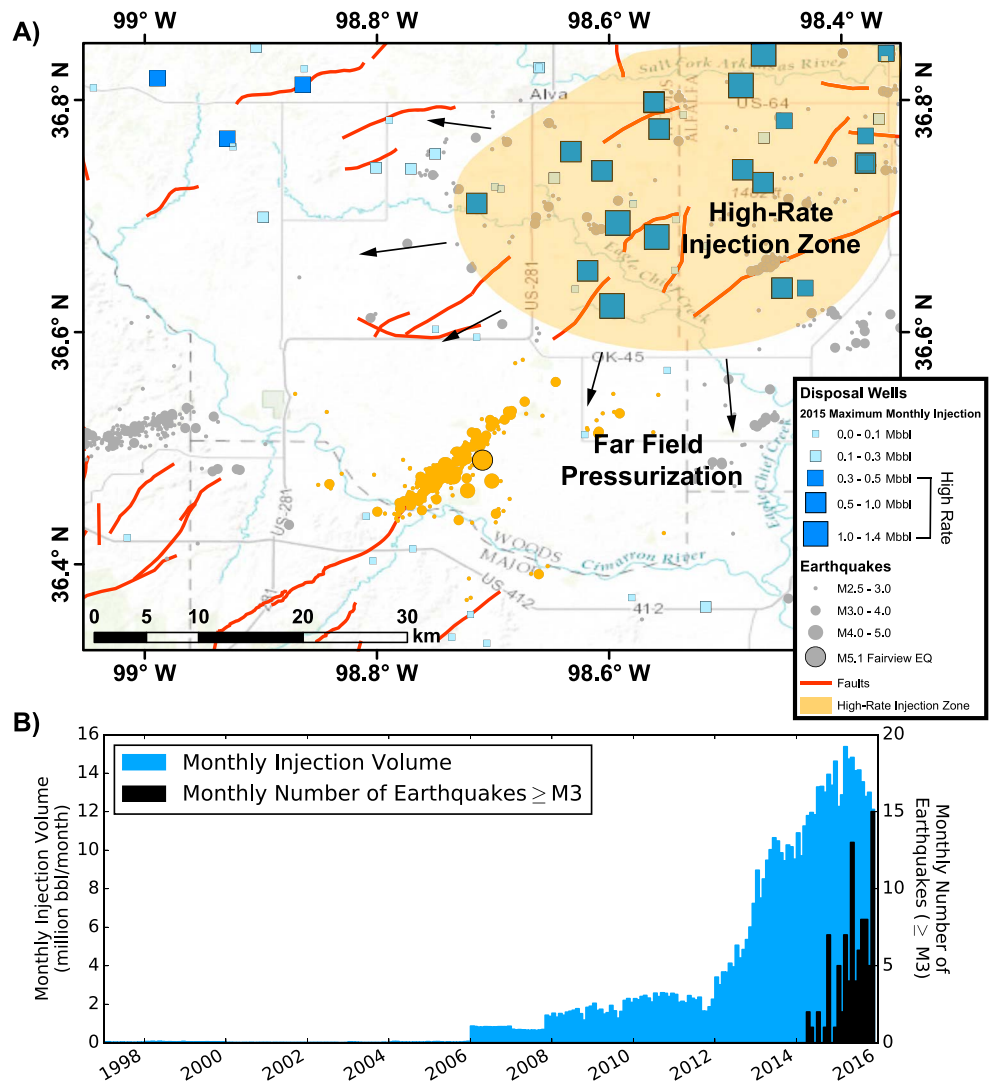


Figure 1. (a) Overview of the Fairview region. Class II injection wells in the region (latitude: 36.326, 36.849; longitude: $-99.053, -98.349$) are shown as blue squares, sized according to maximum injection rate in 2015. Gray circles denote earthquake epicenters in the region from 1 January 2013 to 1 May 2016, with orange circles denoting the Fairview sequence relocated in this study. NEIC reported single-event locations shown in Figure 2. Black arrows show schematic of the pore-pressure diffusion from high-rate wells. Red lines are known faults [Holland, 2015]. (b) Cumulative monthly injection rate of 79 wells operating in the Fairview sequence region (shown in Figure 1a) shown in blue. For the same region, monthly count of earthquakes $M3$ or greater in USGS COMCAT is shown in black.

earthquakes (Figure S1 in the supporting information). Three $M_w 4$ and greater earthquakes ($M_w 4.4, M_w 4.7$, and $M_w 4.4$) occurred within a 4 h period on 7 January 2016, with a summed moment equivalent to that of a $M_w 4.9$ earthquake.

2. Methods

2.1. Calibrated Multiple Earthquake Relocations

We use the hypocentroidal-decomposition (HD) multiple-event relocation algorithm [Jordan and Sverdrup, 1981] to improve upon USGS National Earthquake Information Center (NEIC) single-event relocations. The HD method minimizes bias in event locations, using data to constrain both absolute and relative locations and their associated hypocentral uncertainties. The HD method has been used extensively by NEIC to create calibrated earthquake catalogs in a variety of tectonic settings [Hayes et al., 2013, 2014; Barnhart et al.,

2014; McNamara *et al.*, 2014, 2015a]. HD separates the multiple-event relocation into two independent inversions; one locating earthquakes in a cluster relative to their hypocentroid and one locating the hypocentroid in an absolute sense. In order to estimate calibrated locations, we locate the hypocentroid using only near-source observations (within 0.8°) thereby reducing bias introduced by unmodeled velocity structure and removing any issues introduced through inaccurate phase labeling near the Pg/Pn crossover. Our velocity model was a modification of a model created to relocate events in the Prague, Oklahoma, earthquake sequence [McNamara *et al.*, 2015a] and is primarily based on the western U.S. (WUS) velocity model [Herrmann *et al.*, 2011] (Table S1). We use arrival-time observations at distances up to 3 degrees to solve for cluster vectors (defining locations and origin times relative to the hypocentroid), as relative locations computed from differential times are less sensitive to bias introduced by velocity models [Wolfe, 2002].

Using the HD method with P- and S-wave arrival times we obtain high-precision epicentral locations for 575 earthquakes in the sequence, with precise hypocenter estimates for 367 aftershocks detected after the local deployment of seismic stations. Prior to the local deployment directly following the February 13, 2016, event, there were no seismic stations closer than 25 km from the M_w 5.1 epicenter making it difficult to compute accurate earthquake source depths from arrival-time data alone. For 10 significant earthquakes, prior to the local deployment, independent source depths were determined from regional moment tensors analysis. Hypocenter-free depths were also estimated for these events by tying them to the HD relocation cluster of events during the local deployment. Constraining depth for large events is especially important, as depth is a key factor in understanding generated ground motions and stress-drop variations of induced earthquakes.

2.2. Regional Moment Tensor Solutions

We were able to compute regional moment tensor (RMT) solutions for 27 earthquakes using the procedure outlined by Herrmann *et al.* [2011] (see acknowledgments and data). RMT analysis provides an estimate of the strike, dip, and rake of the nodal planes, seismic moment, and depth of the best-fitting solution. RMT processing was primarily done in the pass band of 16–50 s but modified slightly to shorter periods for smaller events (typically 10–33 s). We use the WUS velocity model [Herrmann *et al.*, 2011], which predicts well Pg, Pn, Sg, and Sn traveltimes and observed surface-wave group velocities in the pass band of interest.

2.3. Stress Modeling

We compute the Coulomb failure stress change (Δ CFS) of the February M_w 5.1 earthquake in an effort to better understand the primary rupture zone of the event in the context of its aftershocks. In order to estimate the Δ CFS imposed from this event, we convert the regional moment tensor solution to uniform slip on a rectangular finite fault, following Herman *et al.* [2016]. The fault dimensions are inferred from empirical relationships between earthquake size and fault dimensions for subsurface strike-slip faults [Wells and Coppersmith, 1994]. Given the modeled moment of the earthquake and a circular crack model [Eshelby, 1957], a stress drop of ~ 0.4 MPa is implicitly assumed in the Δ CFS modeling. Under the assumption that the event occurred in an elastic and isotropic half space, we are able to calculate the change in the stress field from the event following the analytical expressions of Okada [1992]. We calculate the Δ CFS for a right lateral target fault matching the average primary fault plane inferred from RMT solutions at a depth of 7.5 km, near to the average of the depth of precise aftershock hypocenters. We compute the percentage gain of positively stressed aftershocks with respect to a control set of foreshock earthquakes [e.g., Hayes *et al.*, 2013] to test whether aftershocks occur more frequently in regions of positive Δ CFS as compared to historical seismicity of the sequence. To compare the rupture area delineated by aftershocks to the predicted rupture areas as a function of stress drop, we assume the circular crack model of Eshelby [1957].

3. Seismic Characteristics of the Fairview Sequence

Precise earthquake relocations in the Fairview sequence delineate a fault striking approximately 40° northeast (Figure 2a and Table S2), which is consistent with right-lateral strike-slip faulting as observed in the RMT solutions (Figure 2a). Given the regional ENE maximum horizontal stress in the region, a strike-slip fault of this orientation was previously considered either optimally oriented [Holland, 2013b] or “moderately” optimally oriented to slip [Darold and Holland, 2015]. The Fairview sequence seismicity overlaps approximately 3 km of a previously cataloged northeast-trending fault [Holland, 2015] (Figures 1a and 2a) and extends northeast an additional 11 km beyond the mapped extent of this fault. Extending the length of

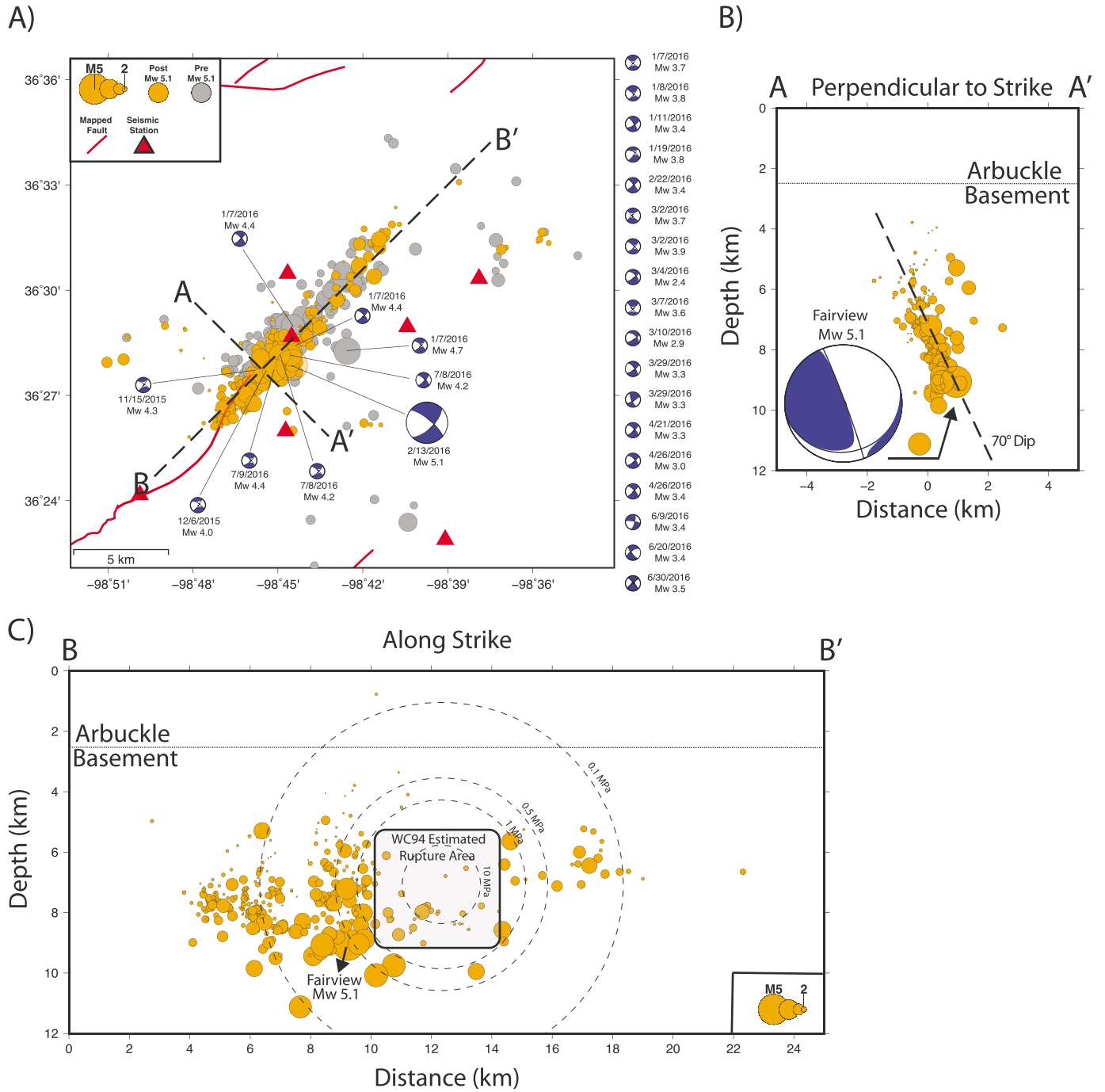


Figure 2. (a) Relocated earthquakes in the Fairview sequence (April 2013 to 1 May 2016) are shown in map view as circles, including earthquakes prior to the 13 February M_w 5.1 event (gray) and those after (orange). Locally deployed USGS stations [ASL/USGS, 1980] are shown as red triangles. Regional moment tensor solutions are shown for events greater and equal to M_w 4.4, connected by a solid black line to the relocated earthquake location. Locations of cross sections shown in Figures 2b and 2c are marked as dotted lines. Mapped Oklahoma faults are shown in red [Holland, 2015]. Off map other regional moment tensors shown. (b, c) Cross sections of relocated aftershocks of the 13 February M_w 5.1 earthquake with good depth controls. Profile locations are shown in Figure 2a. Dotted black line shows approximate depth to basement. (Figure 2b) A cross-sectional profile perpendicular to strike of the inferred fault that shows the dip of fault. The average dip of RMT solutions is shown as a dashed line. The profile view of the RMT for the 13 February M_w 5.1 is shown. (Figure 2c) A cross-sectional profile along strike of the inferred fault. The empirically estimated rupture area of the fault is shown as gray shaded region [Wells and Coppersmith, 1994]. Circular crack sizes given assumed stress drops are shown as black-dashed lines [Eshelby, 1957].

the known fault trace has direct implications on the hazard imposed by this sequence, because, while event nucleation of induced earthquakes may be controlled by injection, maximum magnitudes may have tectonic controls [van der Elst et al., 2016]. The ramification of extending the understood length of a near optimally oriented fault is to increase the potential hazard imposed by the sequence.

Earthquakes clearly delineate an approximately 70° southeast-dipping fault structure, consistent with the RMT modeled dip of the inferred nodal plane of the 13 February M_w 5.1 earthquake (Figures 2a and 2b). Earthquake source depths show that most of the seismicity occurs in the basement at depth of 6–9 km below mean sea level, roughly 3.5–6.5 km below the Arbuckle-Precambrian interface (~2.5 km) [Campbell and Weber, 2006]. The relocated depth of the 13 February M_w 5.1 is 9.1 ± 1.0 km, placing the largest event in the sequence at the base of the seismicity (Figures 2b and 2c). This observation is in accordance with the idea that larger earthquakes nucleate at greater depth [Das and Scholz, 1983], possibly due to an increase in shear resistance and strain energy with depth [Sibson, 1982]. Once an event nucleates in a region of relatively high shear resistance, it is able to rupture the shallower, lower shear-resistant updip portions of the fault [Lapusta et al., 2000].

Relocated hypocenters are in good agreement with RMT solutions. Our preferred rupture plane for the RMT solution for the 13 February M_w 5.1 earthquakes has a strike of 48° and a dip of 70°. The average preferred strike and dip of our RMT solutions is 46° and 79°, respectively. While the slight variation in the inferred strike of the causative fault between the hypocenter observations (40°) and RMT solutions (46°) may be partially a result of bias from unmodeled seismic velocity structure, the inferred strike and dip in the RMT solutions is more consistent with an optimally oriented fault structure [Holland, 2013b; Darrold and Holland, 2015].

While seismicity is occurring on an approximately 14 km long fault segment in the crystalline basement, the majority of aftershock seismicity occurs on a 6 km long portion of the fault, primarily southwest of the M_w 5.1 epicenter. Northeast of the main shock, there is a decrease in seismicity for approximately 4 km to the northeast of the M_w 5.1 earthquake (Figure 2c). After this aseismic zone, there is a slight increase in $> M_{2.5}$ seismicity on the northeasternmost portion of the active fault structure (Figures 2a and 2c). The aseismic zone seen in Figure 2c may represent the primary rupture area of the 13 February M_w 5.1 events, as aftershocks are commonly observed surrounding major slip patches [e.g., Beroza and Zoback, 1993]. The spatial distribution of seismicity suggests that the M_w 5.1 earthquake ruptured to the northeast, with seismicity to the southwest and northeast of this rupture patch being a response to stress loading near the ends of the rupture plane. A rupture area of 14.8 km² (3.9 km × 4.1 km) is predicted for a strike-slip earthquake of this size [Wells and Coppersmith, 1994], which is consistent with the observed aseismic region (Figure 2c).

Modeling Δ CFS from the M_w 5.1 Fairview event in relation to aftershock locations is consistent with rupture occurring within this aseismic zone (Figure 3). Due to the stress change imposed by the rupture of the M_w 5.1, it is expected that aftershock locations should correspond with positive Δ CFS. Modeling Coulomb stress change for relatively small earthquakes is often reliant on RMT solutions, as finite fault models are difficult to constrain. Without a finite fault model, it is common to assume that a hypocenter location is the center of the fault rupture zone [e.g., Herman et al., 2016]. If we center the rupture zone of the Fairview main shock around its relocated hypocenter, we observe a 20% gain in positively Coulomb stressed aftershocks as compared to prior seismicity, with many aftershocks occurring in regions of negative Δ CFS (Figure S2). If we instead assume aftershocks delineate the rupture zone, we observe a 20% decrease of positively stressed aftershocks (Figure S2). Our preferred model is that the aseismic region of aftershocks northeast of the 13 February 2016, M_w 5.1 earthquake represents the rupture zone, and that its relocated hypocenter marks rupture initiation on the downdip, southwestern edge of the rupture zone. This rupture scenario results in a 32% gain of positively Coulomb stressed aftershocks (Figures 3 and S2) and therefore is the best fit of these three scenarios.

Given this rupture scenario, we can evaluate the spatial-temporal evolution of the Fairview sequence. A single $M_{2.4}$ earthquake was reported in the Oklahoma Geological Survey earthquake catalog in 2005 (see acknowledgments and data). The sequence primarily began in mid-2013 with limited seismicity through most of 2015. The first M_w 4 earthquake occurred in November 2015, marking an increase in seismicity along the fault. In early 2016, seismicity began to occur partially in the region we interpret as the rupture zone of the M_w 5.1 earthquake (Figures 2 and S3). This suggests that foreshocks to the M_w 5.1 event were partially delineating the future rupture location of the earthquake. We compare the inferred rupture area of the M_w 5.1 to the circular crack size

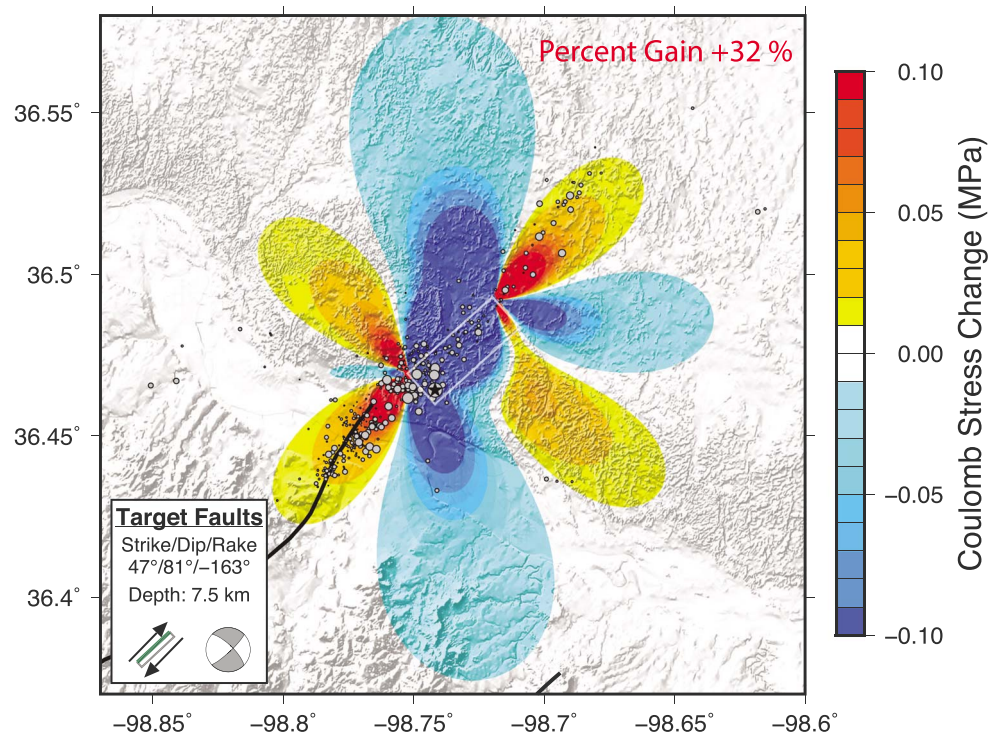


Figure 3. Coulomb failure stress change (Δ CFS) models from the rupture of the 13 February M_w 5.1 earthquake for our preferred rupture scenarios shown. Fault geometry and magnitude estimated from regional moment tensor solution. Fault size estimated using the relationships of Wells and Coppersmith [1994]. Aftershocks are shown as gray circles. Mapped faults shown as black lines [Holland, 2015].

predicted given the estimated moment release from the RMT for a range of stress drops (Figure 3b). A stress drop range of 0.5–1.0 MPa fit our observations.

3.1. Potential Anthropogenic Sources of Sequence

3.1.1. Wastewater Injection

Class II wastewater disposal in the Fairview region (defined in Figure 1) began as early as the mid-1990s (Figure 1), though it is possible that disposal occurred earlier, as records prior to the mid-1990s are incomplete. In the early years of reported injection, fewer than 10 wells operated in the ~ 3600 km² region. Through the end of 2005, the combined monthly injection rate of all disposal wells in the region was low, staying below 81,000 barrels per month. From the beginning of 2012 through the beginning of 2015, injection increased sevenfold, rising from approximately 2.2×10^6 bbl/month to 15.3×10^6 bbl/month (Figure 1b). Injection expanded to 58 wells in the Fairview region (defined in Figure 1) in 2015 with nearly 90% of all injection occurring at 26 high-rate wells (Figure 1a). Five of these high-rate wells had monthly rates of injection exceeding 1×10^6 barrels per month in 2015 (Figure 1a).

While the five closest injection wells, operating between 8 and 12 km from the main shock epicenter, all had average rates less than 35,000 bbl/month in 2015, the temporal onset of regional high-rate injection correlates well with the onset of seismicity in the Fairview sequence. Most wastewater injection wells in the region operate in the deepest sedimentary stratigraphic unit, the Arbuckle Group [Morgan and Murray, 2015]. High-rate injectors typically operate at very low injection pressures in the Arbuckle, mostly between 0 and 2 MPa when accounting for wellbore friction, indicating high-reservoir permeability and the potential to transmit fluid pressure over great distances [Oklahoma Corporation Commission Imaging Web Application, 2016]. In addition, the Arbuckle Group is likely hydraulically connected to the Precambrian basement through permeable fractures and faults as has been shown in other regions of Oklahoma with similar stratigraphy [Keranen et al., 2014]. Assuming reservoir hydraulic diffusivities in the range between 1 and 10 m²/s, the sevenfold increase in the region's injection rates by mid-2014 could produce fluid pressure changes 12+ km away by middle to late 2015. This range is typical of hydraulic diffusivities worldwide and within Oklahoma in regions of

induced seismicity [Talwani *et al.*, 2007; Keranen *et al.*, 2014]. The timing of the ramp up in the Fairview region's injection rates, and reasonable temporal delay under the observed spatial distance, suggests that wastewater injection may have triggered the Fairview sequence, including the M_w 5.1 13 February 2016 Fairview main shock. This spatiotemporal correlation is strong evidence for injection as the anthropogenic source of these earthquakes when combined with one of the known causal mechanisms of induced seismicity: the reduction of effective stresses on preexisting faults [Ellsworth, 2013]. Hydromechanical modeling may be used to further evaluate effective stress changes in the Fairview region.

Under the assumption that Fairview seismicity was tied to these distant injectors, the Oklahoma Corporation Commission (OCC) took action to reduce injection rates. Following the 7 January sequence of three $M_w > 4$ earthquakes, OCC implemented a reduction in injection rates on average by 18% for 27 wells in the Fairview Region (see acknowledgments and data). The wells affected by this reduction primarily were located 15 km or greater away from the Fairview sequence to the northeast. The OCC based this order in part on the suggestion that the January seismicity may have occurred in response to a spike in Arbuckle injection following power restoration after an outage caused by an ice storm during the week of 4 January 2016 (see acknowledgments and data).

Given that the distance between most injection wells and earthquakes ranged from 8 to 30 km, and given that there was a delay of only a few days between earthquakes and the power restoration, we compute the required hydraulic diffusivities to affect fluid pressures in the area of the Fairview earthquakes. Calculated diffusivities between 250 and 3500 m²/s would be required for the power outage-related spike in injection to have significantly influenced the earthquake region. This calculated range of diffusivities is ~1–3 orders of magnitude greater than the largest diffusivities observed in the majority of previous case studies of induced seismicity referenced above [Talwani *et al.*, 2007]. Hence, we conclude that changes in operational parameters during and after the power outage are unlikely to be responsible for the earthquake sequence. This also leads us to conclude that sporadic daily variation in well operations did not have a prominent effect on seismicity rates in the sequence. Instead, the longer-term monthly to annual operation of these wells is the key factor in increasing pore pressures at depth.

3.1.2. Hydraulic Fracturing

We examined spatial-temporal data on hydraulic fracturing operations in the Fairview region to assess any potential correlation. Hydraulic fracturing stimulation typically involves injection over several hours up to several days and is significantly smaller in total injected volume than typical wastewater injection [Rubinstein and Mahani, 2015; Lee *et al.*, 2016]. Case studies of hydraulic fracturing induced-seismicity show earthquakes typically occur within 1–2 km in plan view and either during stimulation period or up to hours to days after the stimulation [Holland, 2013a; Friberg *et al.*, 2014; Skoumal *et al.*, 2015].

From 1 January 2015 to 1 May 2016, nearly 200 hydraulic fracturing stimulations were carried out in the Fairview region (Figure S4). No stimulation occurred within 8 km of the Fairview main shock epicenter at any time in the year prior to rupture (Figure S4a). In the 2 months leading up to rupture, no stimulations occurred within 17 km of the main shock epicenter, and the closest operation on the day of rupture was 26 km away (Figure S4b). Based on close spatial and temporal relationships observed in other sequences linked to hydraulic fracturing, we conclude there is no evidence of a correlation between hydraulic fracture stimulation and the Fairview sequence.

3.1.3. Production

Hundreds of gas production wells are located in the Fairview region (Figure S5), primarily producing from the Oswego and Mississippi Lime formations (informal names [Murray, 2015]) that are stratigraphically shallower than the Arbuckle injection interval. While production wells appear spatially correlated with Fairview seismicity, there are a few distinguishing features that make it unlikely that gas production significantly contributed to the induced sequence. First, gas production peaked in December 2008 and has since declined, currently at its lowest levels since 1998 (Figure S5). Second, the relatively shallow gas extraction would likely require a poroelastic mechanism to induce earthquakes, as a reduction in fluid pressure would increase effective stresses on faults [Segall, 1989]. Production-related poroelastic stress changes depend on their relative location to faults and fault orientations. However, production-related stress changes would be less likely to trigger the strike-slip faults of the Fairview sequence as the mechanism dominantly effects stress changes on normal and reverse faults [Chang and Segall, 2016]. Finally, the lack of seismicity in the 8 years between peak gas production and Fairview seismicity is far too long to suggest a production-related mechanism. The timescale of the

production-related poroelastic mechanism would be much shorter than the observed 8 year delay between peak gas production and Fairview seismicity. Data on oil production in the region were not available at the individual well level for recent years; however, the same mechanistic discussion above applies to oil production. Based on our observations, production in the region is an unlikely trigger for the Fairview sequence.

4. Discussion

It is notable that the Fairview earthquake sequence occurred 12–20 km from high-rate disposal wells, suggesting that the long-term operation of the wells and subsequent far-field pressurization led to effective stress changes necessary to induce these earthquakes. In addition, seismicity directly surrounding high-rate wells to the northeast (Figure 1) is diffuse as compared to the Fairview sequence, hosting no earthquakes of comparable size to the M_w 5.1 Fairview event, even though optimally oriented faults are mapped in the region directly surrounding these wells [Darold and Holland, 2015] (Figure 1a). Assuming a simple, homogeneous permeability structure in the region, it is expected that the maximum pore-pressure perturbation from the high-rate wells would be in their immediate vicinity. We therefore do not observe a correlation between absolute pore-pressure change and large magnitude-induced seismicity. Instead, the fact that the Fairview sequence occurs distant from the wells emphasizes the critical role preexisting geologic structures play in the scale of induced earthquake sequences. The faults near the high-rate wells may be too small to host large events or may be poorly oriented given the state of stress in the crust. Heterogeneous permeability structure can also add to the spatial variability observed in induced earthquake locations [e.g., Hornbach *et al.*, 2016; King *et al.*, 2016]. Because faults are often mapped in sedimentary rocks, do not contain dip information, and many fault characteristics are unknown, it is difficult to determine which distinct traits led to the energetic Fairview seismicity.

The Fairview M_w 5.1 and many of the larger earthquakes in the sequence nucleated near the base of the seismogenic zone (Figure 2c). This observation is similar to that of other large earthquakes in the region. For example, the largest recorded earthquake in Kansas, the induced Milan M 4.9 2014 earthquake, also nucleated near the base of the earthquake sequence [Choy *et al.*, 2016]. Earthquake relocations of the induced 2011 Prague, OK, earthquake show that large events locate deeper in the earthquake sequence, though the depth of the M_w 5.7 was poorly constrained from arrival-time observations [see McNamara *et al.*, 2015a, supporting information]. The potential role event-depth plays in nucleating larger-induced earthquakes warrant further investigation.

5. Conclusions

The 13 February M 5.1 Fairview earthquake is the largest earthquake induced by wastewater injection in Oklahoma since the 2011 M_w 5.6 Prague event and one of the largest earthquake sequences induced by wastewater disposal to date. We find the following:

1. Earthquakes primarily occur in the basement, at depths of 6–9 km, roughly 3.5–6.5 km below the Arbuckle Group in which wastewater injection is occurring throughout the region.
2. Earthquakes occur on a 14 km long segment, partially on a previously unmapped fault segment. The majority of seismicity occurs on a 6 km portion of the fault on its southwestern end. Hypocenter and RMT data show the fault strikes and dips between approximately 40°–48° and 70°–80°, respectively.
3. Aftershocks delineate an aseismic region that may represent the major rupture zone of the M_w 5.1 earthquake. This inferred main shock rupture zone predicts increases and decreases in Coulomb failure stresses that agree with observed aftershock locations.
4. Clustered, high-rate injection 12+ km northeast of the sequence is the most likely anthropogenic source that induced these earthquakes. This conclusion is based on the spatiotemporal correlation between injection and earthquakes combined with the well-known causal mechanism of effective stress change on faults. The Fairview sequence acts as a case example of the far-reaching impact of wastewater injection.

The fact that seismicity is diffuse near the high-rate wells, and the Fairview sequence occurs at a relatively large distance from the wells, points to the critical role preexisting, though possibly unknown, fault structures play in inducing large events. The rapid deployment of seismic stations allowed for the precise relocation of earthquakes. High-quality data sets such as these are crucial when trying to constrain the

Acknowledgments

We thank the seismic analysts at the U.S. Geological Survey (USGS) National Earthquake Information Center for their work documenting this sequence. Thank you to the USGS Albuquerque Seismological Laboratory for their rapid deployment of instrumentation in the Fairview region. Thanks to Austin Holland, George Choy, Cliff Frohlich, and an anonymous reviewer for their insightful reviews of this manuscript. We thank Rob Skoumal for providing data on hydraulic fracture stimulation he compiled from FracFocus in the Fairview region for 2015–2016. This research was supported by the USGS National Earthquake Hazards Reduction Program. M.W. was supported by the Stanford Center for Induced and Triggered Seismicity. All waveform data used in this study are available at the IRIS DMC. Details on the deployed seismic network [Albuquerque Seismological Laboratory (ASL/USGS), 1980] surrounding the Fairview Sequence can be found at <http://www.fdsn.org/networks/detail/GS/>. Details of USGS products regarding the 13 February M 5.1 Fairview earthquake, including magnitude estimations, Did You Feel It reports, shakemaps, and moment tensor solutions, can be found at <http://earthquake.usgs.gov/earthquakes/eventpage/us20004zy8#general> (last accessed 21 May 2016). When applicable, similar data products can be found for all earthquakes reported by the NEIC, whose comprehensive catalog can be accessed at <http://earthquake.usgs.gov/earthquakes/search/> (last accessed 1 June 2016). The Oklahoma Geological Survey earthquake catalog can be found at <http://www.ou.edu/content/ogs/research/earthquakes/catalogs.html> (last accessed 8 September 2016). Details on regional moment tensor solutions can be found at NEIC earthquake event pages and at http://www.eas.slu.edu/eqc/eqc_mt/MECH.NA/ (last accessed 22 June 2016). The Oklahoma Corporation Commission's wastewater injection volume reduction plans following the 7 January Fairview seismicity can be found at <http://www.occeweb.com/News/01-13-16ADVISORY.pdf> (last accessed 14 June 2016). Details on wells drilled to basement in Oklahoma are provided by the OGS at <http://ogs.ou.edu/docs/special-publications/SP2006-1T1.xls> (last accessed 22 June 2016). Information on "Did you Feel It?" data product can be found at <http://earthquake.usgs.gov/data/dyfi/> (last accessed 19 July 2016). Figures 1 and S5 use Ersi World Topographic Map for a base map (sources: Esri, HERE, DeLorme, Intermap, INCREMENT P, GEBCO, USGS, FAO, NPS, NRCAN, GeoBase, IGN, Kadaster NL,

ground motions and stress drops produced by induced events and therefore are an important basis for earthquake hazard modeling.

References

- Albuquerque Seismological Laboratory (ASL/USGS), U.S. Geological Survey Networks International Federation of Digital Seismograph Networks. Other/Seismic Network, doi:10.7914/SN/GS.
- Barnhart, W. D., H. M. Benz, G. P. Hayes, J. L. Rubinstein, and E. Bergman (2014), Seismological and geodetic constraints on the 2011 M_w 5.3 Trinidad, Colorado earthquake and induced deformation in the Raton Basin, *J. Geophys. Res. Solid Earth*, *119*, 7923–7933, doi:10.1002/2014JB011227.
- Beroza, G. C., and M. D. Zoback (1993), Mechanism diversity of the Loma–Prieta aftershocks and the mechanics of mainshock-aftershock interaction, *Science*, *259*, 210–213, doi:10.1126/science.259.5092.210.
- Campbell, J. A., and J. L. Weber (2006), *Wells Drilled to Basement in Oklahoma*, Oklahoma Geological Survey. [Available at <http://www.ou.edu/content/ogs/publications/specialpublications.html>.]
- Chang, K. W., and P. Segall (2016), Seismicity on basement faults induced by simultaneous fluid injection–extraction, *Pure Appl. Geophys.*, *173*, 1–16.
- Choy, G. L., J. L. Rubinstein, W. L. Yeck, D. E. McNamara, C. S. Mueller, and O. S. Boyd (2016), A rare moderate-sized (M_w 4.9) earthquake in Kansas: Rupture process of the Milan, Kansas, earthquake of 12 November 2014 and its relationship to fluid injection, *Seismol. Res. Lett.*, doi:10.1785/0220160100.
- Darold, A. P., and A. A. Holland (2015), Preliminary Oklahoma optimal fault orientations, *Oklahoma Geol. Surv. Open File Rep.*, OF4-2015.
- Das, S., and C. H. Scholz (1983), Why large earthquake do not nucleate at shallow depths, *Nature*, *305*, 621–623.
- Ellsworth, W. L. (2013), Injection-induced Earthquakes, *Science*, *341*(6142), doi:10.1126/science.1225942.
- Eshelby, J. D. (1957), The determination of the elastic field of an ellipsoidal inclusion, and related problems, *Proc. R. Soc. A Math. Phys. Eng. Sci.*, *241*(1226), 376–396, doi:10.1098/rspa.1957.0133.
- Friberg, P. A., G. M. Besana-Ostman, and I. Dricker (2014), Characterization of an earthquake sequence triggered by hydraulic fracturing in Harrison County, Ohio, *Seismol. Res. Lett.*, *85*(6), 1295–1307, doi:10.1785/0220140127.
- Frohlich, C., and S. D. Davis (2002), *Texas Earthquakes*, vol. 2, Univ. of Tex. Press, Austin.
- Hayes, G. P., E. Bergman, K. L. Johnson, H. M. Benz, L. Brown, and A. S. Meltzer (2013), Seismotectonic framework of the 2010 February 27 M_w 8.8 Maule, Chile earthquake sequence, *Geophys. J. Int.*, *195*(2), 1034–1051, doi:10.1093/gji/ggt238.
- Hayes, G. P., M. W. Herman, W. D. Barnhart, K. P. Furlong, S. Riquelme, H. M. Benz, E. Bergman, S. Barrientos, P. S. Earle, and S. Samsonov (2014), Continuing megathrust earthquake potential in Chile after the 2014 Iquique earthquake, *Nature*, *512*, 295–298, doi:10.1038/nature13677.
- Herman, M. W., K. P. Furlong, G. P. Hayes, and H. M. Benz (2016), Foreshock triggering of the 1 April 2014 M_w 8.2 Iquique, Chile, earthquake, *Earth Planet. Sci. Lett.*, *447*, 119–129, doi:10.1016/j.epsl.2016.04.020.
- Herrmann, R. B., H. Benz, and C. J. Ammon (2011), Monitoring the Earthquake source process in North America, *Bull. Seismol. Soc. Am.*, *101*(6), 2609–2625, doi:10.1785/0120110095.
- Holland, A. A. (2013a), Earthquakes triggered by hydraulic fracturing in south-central Oklahoma, *Bull. Seismol. Soc. Am.*, *103*(3), 1784–1792, doi:10.1785/0120120109.
- Holland, A. A. (2013b), Optimal fault orientations within Oklahoma, *Seismol. Res. Lett.*, *84*(5), 876–890.
- Holland, A. A. (2015), Preliminary fault map of Oklahoma, *Oklahoma Geol. Surv. Open File Rep.*, OF3-2015.
- Holland, A. A., C. R. Toth, and E. M. Baker (2013), Probabilistic seismic hazard assessment and observed ground motions for the Arcadia, Oklahoma, dam site, *Oklahoma Geol. Surv. Spec. Pub.*, *1*, 73.
- Hornbach, M. J., M. Jones, M. Scales, H. R. DeShon, M. B. Magnani, C. Frohlich, B. Stump, C. Hayward, and M. Layton (2016), Ellenburger wastewater injection and seismicity in north Texas Physics of the Earth and Planetary Interiors.
- Hough, S. E., and M. Page (2015), A century of induced earthquakes in Oklahoma?, *Bull. Seismol. Soc. Am.*, *105*(6), 2863–2870.
- Jordan, T. H., and K. A. Sverdrup (1981), Telesismic location techniques and their application to earthquake clusters in the south-central Pacific, *Bull. Seismol. Soc. Am.*, *71*(4), 1105–1130.
- Keranen, K. M., H. M. Savage, G. A. Abers, and E. S. Cochran (2013), Potentially induced earthquakes in Oklahoma, USA: Links between wastewater injection and the 2011 M_w 5.7 earthquake sequence, *Geology*, *41*(6), 699–702, doi:10.1130/G34045.1.
- Keranen, K. M., M. Weingarten, G. A. Abers, B. A. Bekins, and S. Ge (2014), Sharp increase in central Oklahoma seismicity since 2008 induced by massive wastewater injection, *Science*, *345*(6195), 448–451, doi:10.1126/science.1255802.
- Kim, W.-Y. (2013), Induced seismicity associated with fluid injection into a deep well in Youngstown, Ohio, *J. Geophys. Res. Solid Earth*, *118*, 3506–3518, doi:10.1002/jgrb.50247.
- King, V. M., L. V. Block, and C. K. Wood (2016), Pressure/flow modeling and induced seismicity resulting from two decades of high-pressure deep-well brine injection, Paradox Valley, Colorado, *Geophysics*, *81*(5), B119–B134.
- Lapusta, N., R. Rice, and G. Zheng (2000), Elastodynamic analysis for slow tectonic loading with spontaneous rupture episodes on faults with rate- and state-dependent friction, *J. Geophys. Res.*, *105*, 23,765–23,789, doi:10.1029/2000JB900250.
- Lee, J. Y., M. Weingarten, and S. Ge (2016), Induced seismicity: The potential hazard from shale gas development and CO₂ geologic storage, *Geosci. J.*, *20*(1), 137–148.
- McNamara, D. E., H. M. Benz, R. B. Herrmann, E. A. Bergman, P. Earle, A. Meltzer, M. Withers, and M. Chapman (2014), The M_w 5.8 Mineral, Virginia, earthquake of August 2011 and aftershock sequence: Constraints on earthquake source parameters and fault geometry, *Bull. Seismol. Soc. Am.*, *104*(1), 40–54, doi:10.1785/0120130058.
- McNamara, D. E., H. M. Benz, R. B. Herrmann, E. A. Bergman, P. Earle, A. Holland, R. Baldwin, and A. Gassner (2015a), Earthquake hypocenters and focal mechanisms in central Oklahoma reveal a complex system of reactivated subsurface strike-slip faulting, *Geophys. Res. Lett.*, *42*, 2742–2749, doi:10.1002/2014GL062730.
- McNamara, D. E., et al. (2015b), Reactivated faulting near Cushing, Oklahoma: Increased potential for a triggered earthquake in an area of United States strategic infrastructure, *Geophys. Res. Lett.*, *42*, 8328–8332, doi:10.1002/2015GL064669.
- Morgan, B. C., and K. E. Murray (2015), Characterizing small-scale permeability of the Arbuckle Group, Oklahoma, *Oklahoma Geol. Surv. Open File Rep.*, OF2-2015, 12 pp., Norman.
- Murray, K. E. (2015), Class II Saltwater Disposal for 2009–2014 at the Annual-, State-, and County-Scales by Geologic Zones of Completion, Oklahoma, *Oklahoma Geol. Surv. Open File Rep.*, OF5-2015, 18 pp., Norman.

Ordnance Survey, Esri Japan, METI, Esri China (Hong Kong), swisstopo, MapmyIndia, © OpenStreetMap contributors, and GIS User Community). Other maps produced using GMT 5 software [Wessel et al., 2013]. Hydraulic fracturing data are available (<http://fracfocus.org/>). Digital elevation model data shown in Figure 3 are available from the USGS. Any use of trade, firm, or product names is for descriptive purposes only and does not imply endorsement by the U.S. Government.

- Okada, Y. (1992), Internal deformation due to shear and tensile faults in a half space, *Bull. Seismol. Soc. Am.*, *82*(2), 1018–1040.
- Oklahoma Corporation Commission Imaging Web Application (2016), [Available at <http://imaging.occeweb.com/>, last accessed July 2016.]
- Petersen, M. D., C. S. Mueller, M. P. Moschetti, S. M. Hoover, A. L. Llenos, W. L. Ellsworth, A. J. Michael, J. L. Rubinstein, A. F. McGarr, and K. S. Rukstales (2016), 2016 one-year seismic hazard forecast for the central and eastern United States from induced and natural earthquakes *Open File Rep.*, doi:10.3133/OFR20161035.
- Petersen, M. D., et al. (2014), Documentation for the 2014 update of the United States national seismic hazard maps, *U.S. Geol. Surv. Open File Rep.*, *2014–1091*, 243 p., 10.3133/ofr20141091.
- Rubinstein, J. L., and A. B. Mahani (2015), Myths facts on wastewater injection, hydraulic fracturing, enhanced oil recovery, and induced seismicity, *Seismol. Res. Letters*, *86*(4), 1060–1067.
- Rubinstein, J. L., W. L. Ellsworth, A. McGarr, and H. M. Benz (2014), The 2001-present induced earthquake sequence in the Raton Basin of northern New Mexico and southern Colorado, *Bull. Seismol. Soc. Am.*, *104*(5), 2162–2181, doi:10.1785/0120140009.
- Segall, P. (1989), Earthquakes triggered by fluid extraction, *Geology*, *17*(10), 942–946, doi:10.1130/0091-7613(1989)017<0942:ETBFE>2.3.CO;2.
- Sibson, R. H. (1982), Fault zone models, heat flow, and the depth distribution of earthquakes in the continental crust of the United States, *Bull. Seismol. Soc. Am.*, *72*(1), 151–163.
- Skoumal, R. J., M. R. Brudzinski, and B. S. Currie (2015), Earthquakes induced by hydraulic fracturing in Poland Township, Ohio, *Bull. Seismol. Soc. Am.*, *105*(1), 189–197, doi:10.1785/0120140168.
- Sumy, D. F., E. S. Cochran, K. M. Keranen, M. Wei, and G. Abers (2014), Observations of static Coulomb stress triggering of the November 2011 *M* 5.7 Oklahoma earthquake sequence, *J. Geophys. Res. Solid Earth*, *119*, 1904–1923, doi:10.1002/2013JB010612. Received.
- Talwani, P., L. Chen, and K. Gahalaut (2007), Seismogenic permeability, *ks*, *J. Geophys. Res.*, *112*, B07309, doi:10.1029/2006JB004665.
- van der Elst, N. J., M. T. Page, D. A. Weiser, T. H. W. Goebel, and S. M. Hosseini (2016), Induced earthquake magnitudes are as large as (statistically) expected, *J. Geophys. Res. Solid Earth*, *121*, 4575–4590, doi:10.1002/2016JB012818.
- Walsh, F. R., and M. D. Zoback (2015), Oklahoma's recent earthquakes and saltwater disposal, *Sci. Adv.*, *1*, 1–9, doi:10.1126/sciadv.1500195.
- Weingarten, M., S. Ge, J. W. Godt, B. A. Bekins, and J. L. Rubinstein (2015), High-rate injection is associated with the increase in U.S. mid-continent seismicity, *Science*, *348*(6241), 1336–1340, doi:10.1126/science.aab1345.
- Wells, D., and K. Coppersmith (1994), New empirical relationships among magnitude, rupture length, rupture width, rupture area, and surface displacement, *Bull. Seismol.*, *84*(4), 974–1002.
- Wessel, P., W. H. F. Smith, R. Scharroo, J. F. Luis, and F. Wobbe (2013), Generic Mapping Tools: Improved version released, *Eos. Trans. AGU*, *94*, 409–410, doi:10.1002/2013EO450001.
- Wolfe, C. J. (2002), On the mathematics of using difference operators to relocate earthquakes, *Bull. Seismol. Soc. Am.*, *92*(8), 2879–2892, doi:10.1785/0120010189.
- Yeck, W. L., A. F. Sheehan, H. Benz, M. Weingarten, and J. Nakai (2016), Rapid response, monitoring, and mitigation of induced seismicity near Greeley, Colorado, *J. Chem. Inf. Model.*, *53*(9), 1689–1699, doi:10.1785/0220150275.